NUMERICAL SOLUTION OF THE REACTION–ADVECTION–DIFFUSION EQUATION ON THE SPHERE

Janusz A. Pudykiewicz, MSC, RPN, e-mail: Janusz.Pudykiewicz@ec.gc.ca

In order to provide an alternative to semi–Lagrangian techniques for the solution of the reaction–advection–diffusion equation, a simple yet accurate Eulerian algorithm build upon the principle of finite volumes has been developed. The set of the considered equations has the following form:

$$\frac{\partial \varphi^k}{\partial t} = -\nabla \mathbf{u}\varphi^k + \nabla \mathbf{K}\nabla\varphi^k + F_{\rm c}^k(\varphi^1, \ldots, \varphi^{N_{\rm s}}), \tag{1}$$

where φ^k is the $k^{\rm th}$ scalar field; $k = 1, \ldots, N_{\rm s}$, $N_{\rm s}$ is number of scalar fields, $\mathbf{u}$ is the three–dimensional velocity field, $\mathbf{K}$ is the diffusion tensor, and $F_{\rm c}^k$ are the functions describing the interactions between scalar fields. In a most general case, $F_{\rm c}^k$ can be written as $\alpha_{klm}\varphi^l\varphi^m + \beta_{kl}\varphi^l$, where α_{klm} and β_{kl} are the kinetic coefficients. The approach adopted here exploits the concept of semidiscretization (Leveque, 2002; page 191); first, the convective and diffusive fluxes in (1) are approximated and then, the resulting set of the Ordinary Differential Equations (ODEs) is solved using the appropriate time stepping algorithm. This methodology has been selected because of both its flexibility with respect to the mesh selection and its inherent ability to represent subgrid-scale processes and discontinuities in the solution.

The method is initially applied on a geodesic icosahedral grid composed of triangles with vertices located on the spherical surface (Fig. 1). The control volume Ω_i associated with the $i^{\rm th}$ node is created by a two step procedure. In the first step, the centers of the triangles and the mid-points of the edges are projected on the surface of the sphere. In the second step, Ω_i is defined as a polygon with the vertices located at the projected points (Fig. 2). Equation (1) is then integrated over Ω_i and from the Green theorem,

$$\frac{d\phi_i^k}{dt} = -\frac{1}{S(\Omega_i)} \int\limits_{\partial\Omega_i} (\mathbf{u}\varphi^k - \mathbf{K}\nabla\varphi^k)\, \mathbf{n}\, dl + \frac{1}{S(\Omega_i)} \int\limits_{\Omega_i} F_{\rm c}^k d\mathbf{r}, \tag{2}$$

where $\phi_i^k = \int_{\Omega_i} \varphi^k(\mathbf{r}, t) d\mathbf{r}/S(\Omega_i)$, $i \in [1, N_{\rm p}]$, $N_{\rm p}$ is the number of nodes, $k \in [1, N_{\rm s}]$, and $S(\Omega_i)$ is the surface of Ω_i. After discretizing of the integral terms, equation (2) can be written in a compact vector form as

$$\frac{d\boldsymbol{\phi}}{dt} = -(\mathbf{I}_{N_{\rm s}} \otimes \mathbf{A}_{\mathcal{D}})\boldsymbol{\phi} + \mathbf{F}(\boldsymbol{\phi}), \tag{3}$$

where $\mathbf{A}_{\mathcal{D}}$ is the sparse matrix representing the advection–diffusion operator, $\mathbf{I}_{N_{\rm s}}$ is the $N_{\rm s} \times N_{\rm s}$ diagonal matrix, $\otimes$ denotes the Kronecker product, $\mathbf{F}(\boldsymbol{\phi})$ is the vector of forcings, and $\boldsymbol{\phi}$ is the vector of the finite volume averages of the scalar fields

$$\boldsymbol{\phi} = [\phi_1^1, \phi_2^1, \ldots, \phi_{N_{\rm p}}^1, \phi_1^2, \phi_2^2, \ldots, \phi_{N_{\rm p}}^2, \ldots, \phi_1^{N_{\rm s}}, \phi_2^{N_{\rm s}}, \ldots, \phi_{N_{\rm p}}^{N_{\rm s}}]^{\rm T}.$$

Depending on the stiffness of the system, the time integration of (3) is performed either with the $4^{\rm th}$ order Runge-Kutta scheme or with the Rosenbrock solver . The monotonicity of the scheme is achieved with the explicit local adaptive dissipation proposed by Shchepetkin and McWilliams (1998). The performance of the advection–diffusion solver is assessed using the suite of standard tests based on the solid body rotation of a cosine hill and a cylinder as well as the multiscale signal as suggested by Smolarkiewicz and Grabowski (1989); see Fig. 3 for sample results. The main conclusion from these tests is that the presented method offers mass conservation, quasi monotonicity and good accuracy. Also, the algorithm is stable for the advection with Courant numbers of the order of 2.5, similarly as in the advection tests on structured meshes reported by Vreudeghill (1993).

In order to fully evaluate the method, the reaction–diffusion system on the sphere was also considered. The comparison of the numerical results to the analytical solution presented by Turing (1952) shows that the method is quite accurate with the maximum error not exceeding 0.01%. The solver was also applied for the integration of the nonlinear chemical kinetics system known as a Brusselator (Prigogine and Lefever, 1968).

The main intended application of the reaction-advection-diffusion solver is the simulation of the chemical constituents in the Earth atmosphere. The scheme described herein can also be easily applied on arbitrary differentiable manifolds and, therefore, it is a good candidate for a simulation of tracer transport for both small and large scale flows. The future work will explore numerical solutions of the shallow water equations on the sphere as well as reactive flows at small scales.

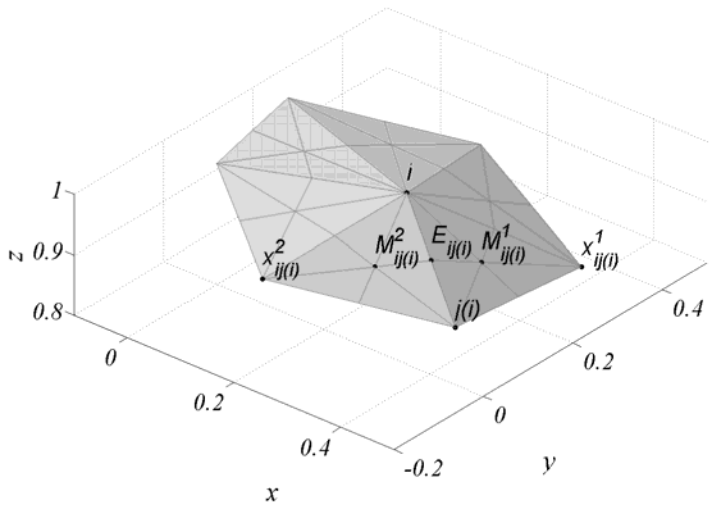

Fig.1 Triangles used in the definition of the finite volumes on the sphere; (i - is the i^{th} node, $j(i)$ - is the node defining one of the incident edges, $E_{ij(i)}$ – is the mid-point of the $(i,j(i))$ edge, $M^l_{i(j(i))}$ – is the mass center of the triangle defined by points: i, $j(i)$, and $x^l_{ij(i)}$ $(l=1,2)$.

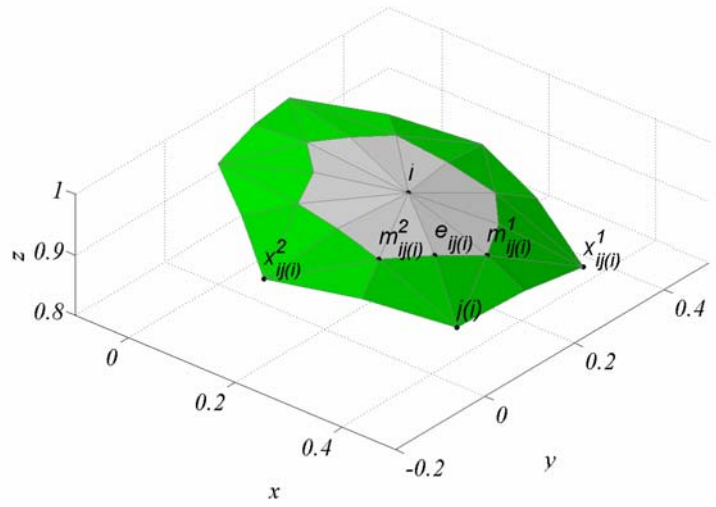

Fig. 2 Finite volume Ω_i (gray polygon); $e_{ij(i)}$, $m^l_{ij(i)}$ denote projected points $E_{ij(i)}$ and $M^l_{ij(i)}$ respectively $(l=1,2)$.

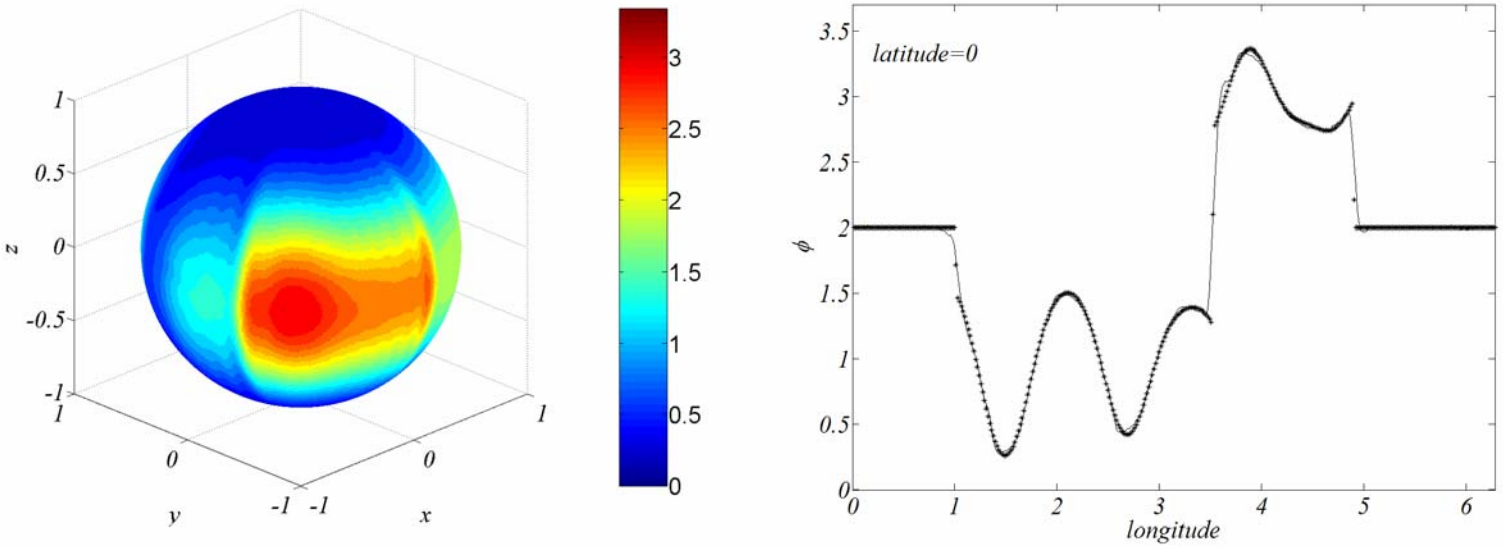

Fig. 3 The solid body rotation of the multiscale signal after one revolution around the equator. The left panel shows results plotted directly on the surface of the sphere whereas the right panel both the analytical solution (dashed line) and the numerical solution (line marked by stars). The initial condition for the test is described by the following function

$$\phi(\theta,\lambda)=\cos^4(\theta)\,(f_1(\lambda)+f_2(\lambda)+2)\left(1+0.3\sin\left(\frac{50}{9}\lambda\right)\right)\left(1+0.4\sin\left(\frac{50}{10}\lambda\right)\right)$$

$$f_1(\lambda)=-1 \text{ for } \lambda\in D_1=[8\pi/25,\,28\pi/25],\quad f_1(\lambda)=0 \text{ for } \lambda\in[0,2\pi]-D_1$$

$$f_2(\lambda)=1 \text{ for } \lambda\in D_2=[28\pi/25,\,39\pi/25],\quad f_2(\lambda)=0 \text{ for } \lambda\in[0,2\pi]-D_2$$

(θ is the latitude and λ is the longitude)

References

Leveque R. J., 2002: Finite Volume Methods for Hyperbolic Problems. Cambridge University Press, Cambridge.

Prigogine I. and R. Lefever, 1968: Symmetry-Breaking Instabilities in Dissipative Systems., J. Chem. Phys., 48, 1695-1700.

Shchepetkin A. and J. C. McWilliams, 1998: Quasi-Monotone Advection Schemes Based on Explicit Locally Adaptive Dissipation. Mon. Wea. Rev., 126, 1541-1580.

Smolarkiewicz P. K. and W. W. Grabowski, 1990: The Multidimensional Positive Denite Advection Transport Algorithm: Nonoscillatory Option. J. Comp. Phys., 86, 355-375

Turing A. M., 1952: The Chemical Basis of Morphogenesis. Phil. Trans. of the Roy. Soc. of London, Series B, 237, 3772.

Vreugdenhill C. B., 1993: Linear Central-Difference Methods. Notes on Numerical Fluid Mechanics; Vol 45, Numerical Methods for Advection-Diffusion Problems, editted by Vreugdenhill C. B. and B. Koren, Braunschweig, Viesbaden, 2754.